Tuijin Jishu/Journal of Propulsion Technology
ISSN: 1001-4055
Vol. 44 No. 5 (2023)

An Innovative Approach to Reduce Bursting and Spalling Stresses at Anchorage Zone of Post-Tensioned Member Incorporating Different Types of Reinforcement Configuration

[1]Manan N. Patel, [2]Nirpex A. Patel, [3]Vijay R. Panchal

[1] Air Product India Pvt. Ltd., Notus IT Park, Sarabhai Campus, Gorwa Road, Vadodara
Email: patelm16@airproduct.com
[2][3] M. S. Patel Department of Civil Engineering, Chandubhai S. Patel Institute of Technology, Charotar University of Science and Technology, Changa, Gujarat, India

Abstract—The intricacies inherent in comprehending stress distribution within the proximity of the termination section of a post-tensioned member, specifically the anchorage zone, underscore the need for precise and viable assessment methods for regions susceptible to heightened stress levels. This study presents a meticulous approach for evaluating anchorage zone stresses, particularly bursting and spalling stresses, utilizing three-dimensional stress distribution using FE analysis employing the ABAQUS program. The effectiveness of the finite element model was verified through a mesh sensitivity analysis. In the evaluation of anchorage zone stresses, multiple anchorage zone reinforcement configurations were meticulously modeled, encompassing distribution ratios (the ratio of the depth of the anchor plate to that of the anchorage zone) spanning from 0.2 to 0.9. This comprehensive analysis facilitated the examination of stress variations, specifically bursting and spalling stresses, across the span of the anchorage zone. Various attempts were made to mitigate these stresses, employing innovative reinforcement configurations, which were systematically compared with conventional counterparts. The outcomes of this study distinctly illustrate that regions experiencing excessive stress levels are efficiently managed with the implementation of suitable reinforcement configurations. The results demonstrate that both bursting and spalling stresses can be effectively controlled in post-tensioned specimens' anchorage zones, achieving reductions of 62% and 33%, respectively, through the strategic deployment of proposed advanced reinforcement configurations.

Index Terms—Prestressed Structures, Post-tensioned anchorage zone, bursting stress, spalling stress, reinforcement configuration, ABAQUS

1. INTRODUCTION

In contemporary engineering practices, prestressing techniques are prominently employed to achieve expansive spans with minimal self-weight and rapid construction timelines. Prestressing concrete is executed through two methodologies: pre-tensioning and post-tensioning. Pre-tensioning involves applying prestress to concrete by tensioning the tendon before concrete placement, relying on the concrete-tendon bond for prestress transfer. Conversely, in post-tensioning, prestress is induced by tensioning tendons against hardened concrete. This method generates significant stress concentration near the end of post-tensioned members, making them susceptible to various transverse stresses such as bursting, spalling, and compressive forces. This specific segment of post-tensioned members is designated as the 'Anchorage zone,' 'End zone,' or 'End block' [1]. Exceeding permissible stress limits in this zone leads to the formation and propagation of cracks, evident in Fig. 1 [2]. To counteract crack development and propagation, appropriate reinforcement configurations are imperative.

Fig 1: Cracks in anchorage zone for single and multiple tendon anchorages [2]

In recent decades, researchers have explored diverse methodologies, including elasticity theory, experimental studies, finite-element analysis, and the strut-and-tie model, to assess post-tensioned anchorage zone stresses, leading to numerous findings.

Mathematical scrutiny of the post-tensioned anchorage zone was conducted [3], yielding a table detailing zero and maximum bursting stress magnitude and position, alongside the introduction of partitioning and equivalent prism concepts for multiple and eccentric cables. Yettram and Robbins [4-5] utilized Finite Element Analysis (FEA) to assess anchorage zone stresses, exploring the variation in bursting stress concerning a wide range of distribution ratios in both two- and three-dimensional stress analyses. Further studies delved into eccentric and multiple anchorages using the equivalent prism technique proposed by Guyon [3], confirming the existence of spalling stress. Iyengar and Yogananda [6] employed a three-dimensional stress distribution approach, idealizing a circular concrete beam with a co-axial duct and presenting stress results in radial and hoop stresses.

Experimental work by Zeilinski and Rowe [7] involved concrete prismatic specimens with surface-strain measurements, investigating parameters like distribution ratio, cable duct, anchorage type, cracking, and ultimate load. Their study indicated that anchorage zone was minimally affected by factors such as anchorage type, material, and wire anchoring method. Gupta and Khapre [8] derived an equation incorporating Poisson's ratio, analyzing the anchorage zone as a two-dimensional plane stress problem using finite element methods on the PARAM 10000 supercomputer platform, highlighting discrepancies with the IS: 1343 [9] equation. He and Liu [10] formulated a formula considering eccentricity, tendon inclination, prestress force, anchor plate depth, and anchorage zone height, achieving accuracy comparable to elastic FEA and experimental results.

Recent numerical analyses by Zhou et al. [11] investigated crack behavior in the anchorage zone specimens, focusing on parameters like crack formation, propagation, first cracking load, crack width, length, trace, and ultimate load. Their research suggested that optimal bar diameter and spacing reduced crack width. Additionally, Zhou et al. [11] developed an advanced elastic to plastic strut-and-tie model to examine the anchorage zone's behavior elastically and inelastically. Similar research by Hou et al. [13] involved formulating a strut-and-tie model for post-tensioned anchorage zone design, analyzing stress distribution using the 'ANSYS 10.0' FEA software.

The necessity arises for a technique that effectively measures anchorage zone stresses and recommends optimal reinforcement, comparing stresses generated by various reinforcement configurations. This study, therefore, focuses on the three-dimensional stress distribution of the post-tensioned anchorage zone, utilizing ABAQUS program to assess zones with distribution ratios *(M)* ranging from 0.2 to 0.9. The study is restricted to a single, concentric, and normal prestress load applied on the anchor plate, replaced by equivalent prestress stress. Notably, this investigation has identified regions highly prone to excessive stress, prompting the implementation of suitable reinforcement configurations to mitigate these stresses. Multiple anchorage zone models were developed, featuring constant distribution ratios (*M*) and prestress loads, incorporating various

reinforcement configurations, including Mats, grids, Links, Loops, Hair-pin bars, and Helix or Spiral [1], alongside proposed RCs 1-9. The results yielded promising outcomes, leading to valuable conclusions.

2. Stresses at Anchorage Zone

A. FE Model

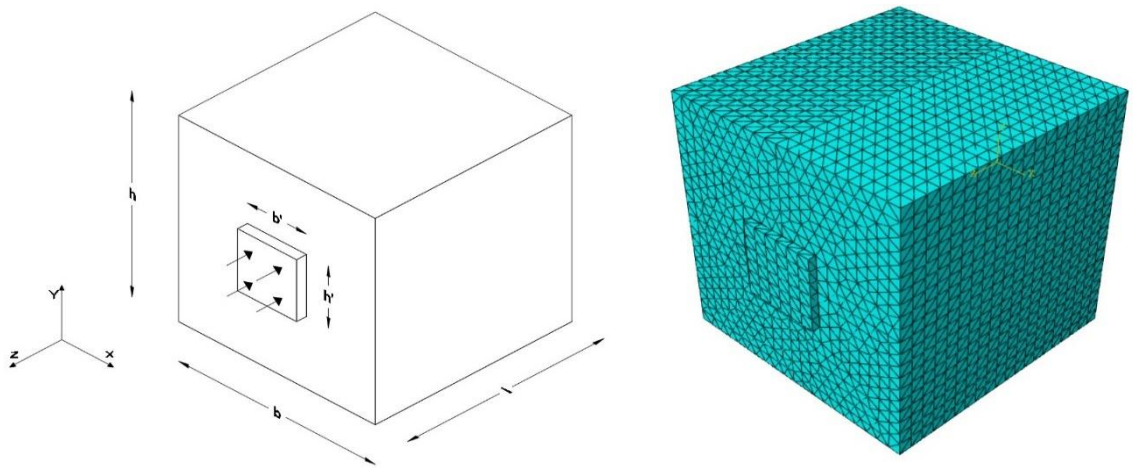

(a) (b)

Fig 2: (a) Geometry of finite element model (b) Meshing of FEM for 3-dimensional anchorage zone

The assessment of the post-tensioned anchorage zone is conducted through a non-linear three-dimensional stress distribution idealization. FE analysis is performed on the anchorage zone, considering a pre-cracking state and excluding the influence of micro-cracks for the current study. For the sake of simplicity, the presence of a cable duct is omitted in this analysis. ABAQUS software is employed to simulate the anchorage zone. The models consist of cubical concrete blocks, with varying distribution ratios *(M)* ranging from 0.2 to 0.9. The size of the anchor plate governs the stress distribution, and a square steel anchor plate is utilized, as depicted in Fig. 2, detailing the anchorage zone geometry. Material properties for concrete and steel, concerning both the anchorage zone and the anchor plate, are outlined in Tables I and II respectively. To effectively transfer the substituted equivalent prestress stress from the anchor plate to the anchorage zone, surface-to-surface interaction ties are applied between them. The entire model is discretized using C3D10 elements, specifically a 10-node quadratic tetrahedron, with an element size of 0.05*h*, as illustrated in Fig. 2. To analyze stress variations concerning the anchor plate size, a consistent prestress force is maintained across all anchorage zone models, subsequently replaced by an equivalent stress calculated by dividing the prestress force by the anchor plate area. A support structure is implemented on the back face opposite to the loaded face, offering displacement restraint solely in the loading direction.

Table I: Material Properties of Concrete

Density (Tonne/mm^3)	2.3×10^{-9}
Elastic: Young's modulus (N/mm^2)	3×10^4
Poisson's ratios (μ)	0.18 0.125 0.2 0.45

TABLE II: MATERIAL PROPERTIES OF STEEL (ANCHOR PLATE)

Density (Tonne/mm^3)	7.85×10^{-9}
Elastic: Young's modulus (N/mm^2) Poisson's ratio (μ)	 2.1×10^5 0.3
Plastic: Yield stress (N/mm^2) 250 500	Plastic strain 0 1×10^{-4}

B. Mesh Sensitivity Analysis

Within the framework of this study, mesh sensitivity analysis serves as a vital component for validating the numerical simulations. This process entails methodically refining the computational mesh to assess its influence on the precision and stability of the outcomes. By systematically altering the mesh size within the range of 5000 to 25000 elements and monitoring efficiency variations (0.96 to 1.02) considering μ = 0.125, the reliability of the finite element models is ensured as depicted in Fig. 3. Notably, the finite element model comprising 20,000 mesh elements exhibits an efficiency of approximately 100% concerning bursting stress, aligning closely with the findings of Yettram and Robbins [4]. This meticulously validated model is subsequently employed for further in-depth investigation.

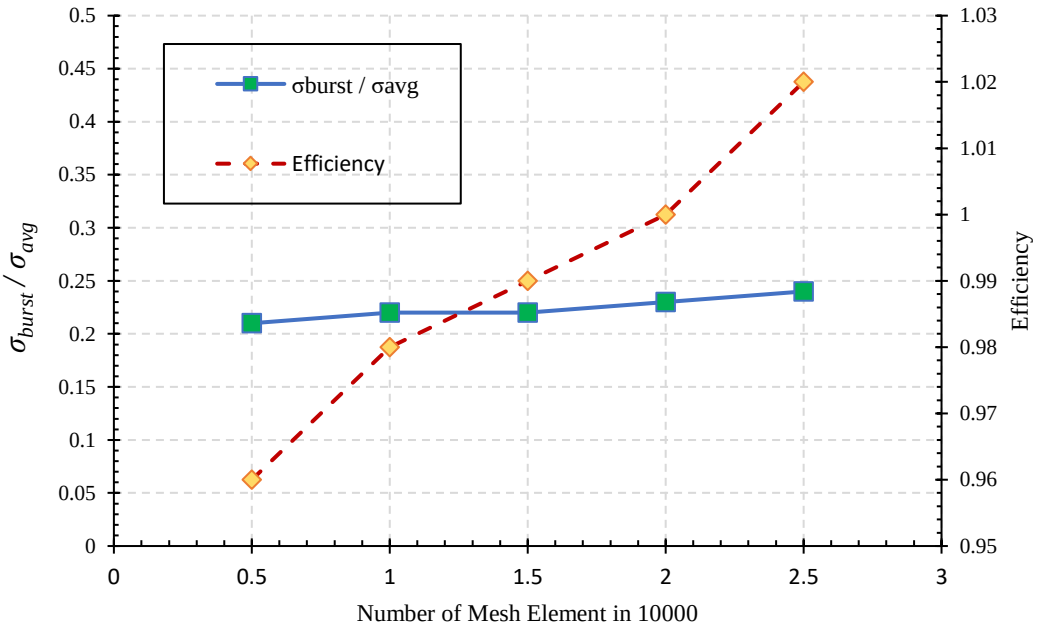

Fig 3: Mesh sensitivity analysis of anchorage zone of in accordance with bursting stress

C. Validation with findings of Yettram and Robbins [4]

In the validation process of the methodology utilized for the assessment of post-tensioned anchorage zone stresses, the results obtained from the Finite Element Analysis using ABAQUS program are meticulously compared with the findings of Yettram and Robbins [4]. Fig. 4 illustrates the transverse tensile stress variation, denoted as bursting stress, along the centroidal axis of the anchorage zone for a typical distribution ratio (M) of 0.5. The analysis incorporates various Poisson's ratios: 0.125, 0.2, and 0.45, respectively. To ensure a stringent comparison with the earlier study, the modeling of this specific anchorage zone is conducted differently, where

the substituted equivalent prestress stress is directly applied on the anchorage zone surface, deviating from the conventional practice of applying it on the anchor plate.

Upon careful analysis of Fig. 4, it is evident that the results from the current study align closely with those of Yettram and Robbins [4] for each Poisson's ratio value, except for μ = 0.45. A marginal discrepancy of 4.35% in peak stress value is observed in the case of μ = 0.45. In contrast, for μ = 0.125 and μ = 0.2, the differences stand at 1.09% and 2.68%, respectively. Importantly, these discrepancies fall well within the acceptable range, considering the concrete Poisson's ratio typically ranges from 0.1 to 0.2. Consequently, the Finite Element Analysis procedure employed for the evaluation of anchorage zone stresses through the ABAQUS software stands validated.

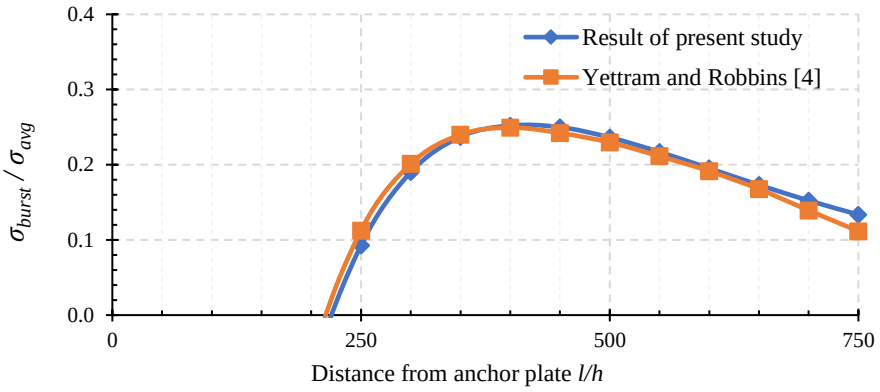

(a) For μ = 0.125

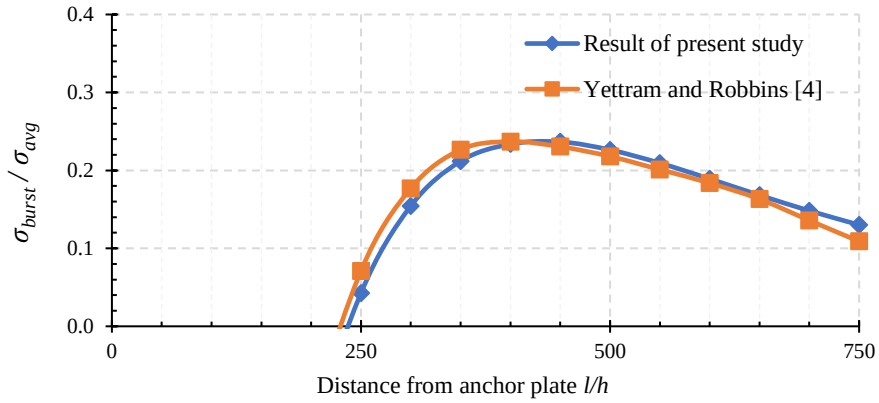

(b) For μ = 0.2

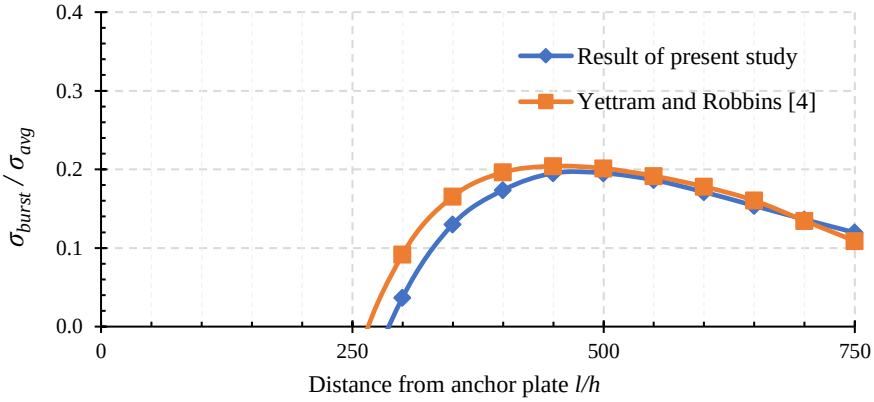

(c) For μ = 0.45

Fig 4: Bursting stress comparison from FEM analysis for M = 0.5 and μ = 0.125, 0.2 and 0.45

D. Stress distribution

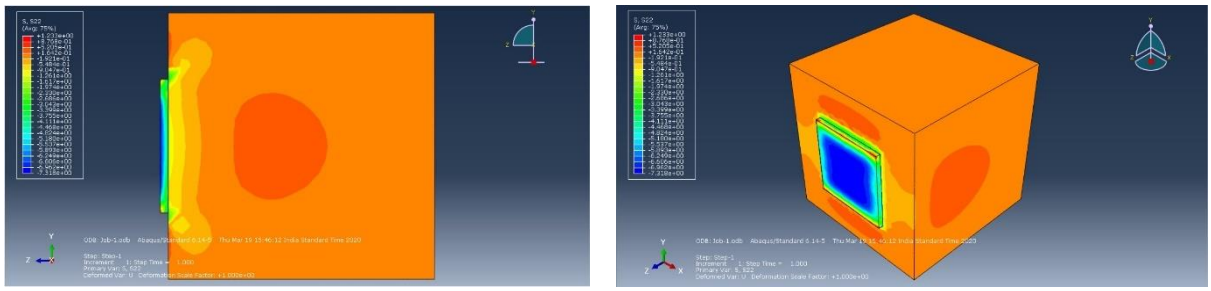

(a) Across vertical plane mid span (b) Whole model

Fig 5: Transverse tensile stress contour in anchorage zone

Fig. 5 provides a comprehensive visual representation of transverse tensile stress distribution resulting from the application of equivalent prestressing stress onto the anchorage zone, specifically for the typical value of M = 0.5. The stress contour displayed in Fig. 5(a) vividly illustrates the development of a distinct zone located at a specific distance from the loading face. This zone emerges due to the lateral dispersion of prestress load from the tendon path, manifesting as the 'bursting stress zone'. Simultaneously, Fig. 5(b) showcases a significant elevation in transverse stress on the loading surface within the neighboring region of the anchor plate, termed the 'Spalling stress zone'. Notably, these stress zones are demarcated by another transverse stress zone, characterized by compressive stress. This zone, known as the 'Compression zone', arises due to the compressive effect exerted by the anchor plate immediately ahead of it, extending over a certain distance along the length of the anchorage zone.

E. Bursting stress

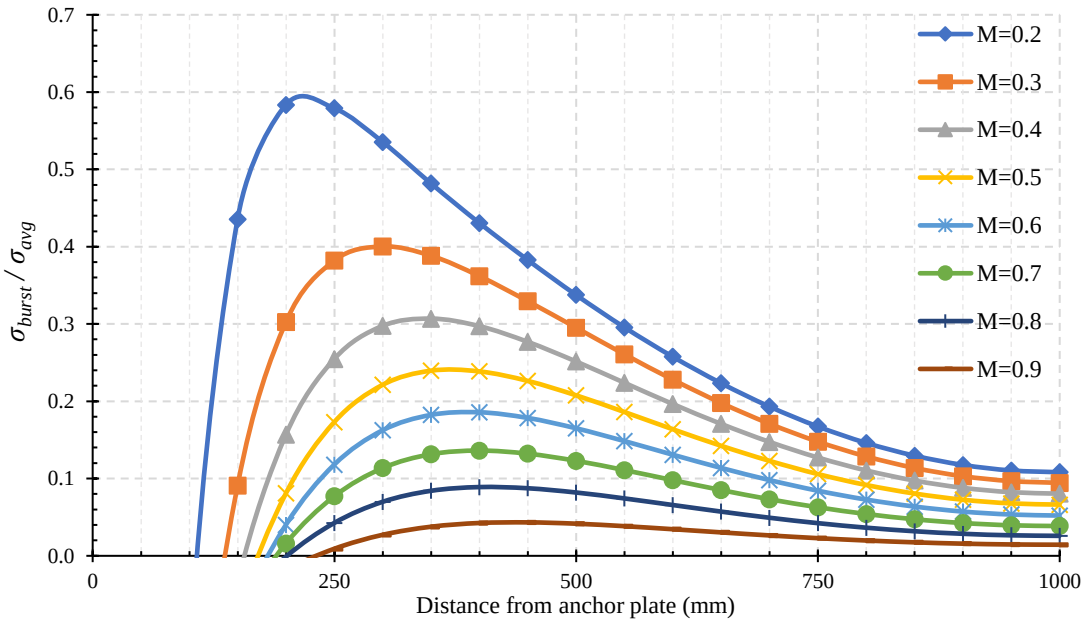

Fig 6: Bursting stress along tendon path with variation in M for μ = 0.18

Fig. 6 illustrates the bursting stress variation along the length of the anchorage zone, acquired on the centroidal axis, considering distribution ratios (M) ranging from 0.2 to 0.9, with a consistent Poisson's ratio (μ) of 0.18. To render this variation universally applicable for non-dimensional parameters, the normalized stress ($\sigma_{burst}/\sigma_{avg}$) and normalized distance (l/h) are utilized on the x and y axes, respectively. For each M value, the bursting stress commences at a specific distance from the loading face and exhibits a sharp increase, reaching its

maximum value, particularly intense for lower *M* values. With increasing *M*, both the position of zero and maximum bursting stress shift ahead of the anchor plate along the loading axis. A gradual decline in bursting stress is observed beyond the peak stress for each *M*. This trend aligns with the bursting stress variation observed by Yettram and Robbins [4] in their comprehensive three-dimensional stress distribution study and corroborated by Gupta and Khapre [8] in their focused two-dimensional stress distribution analysis. Importantly, the total bursting force corresponds to the area enclosed within the specific bursting stress curve, diminishing as *M* increases. Notably, for higher *M* values, the bursting stress remains nearly constant along the entire path.

F. Spalling stress

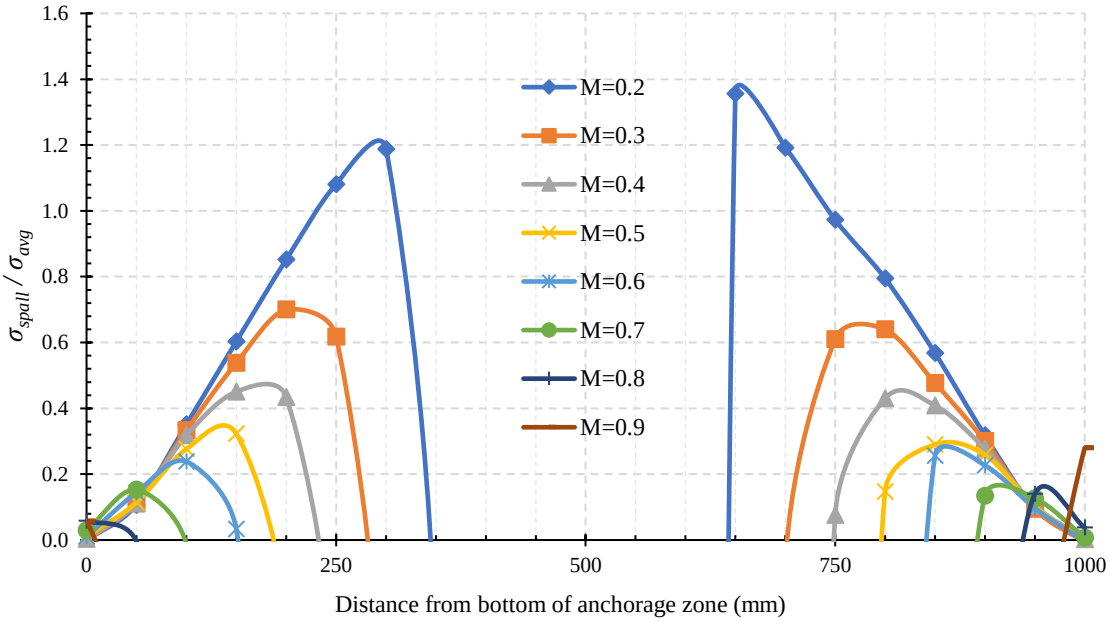

Fig 7: Spalling stress along loading face with variation in M for μ = 0.18

The variation of spalling stress concerning distribution ratio (*M*) is depicted in Fig. 7, offering a clear insight into spalling stress along the vertical centroidal axis on the loading surface (y-axis) for each *M* value. The stress on the y-axis is normalized as $\sigma_{Spall}/\sigma_{avg}$, ensuring a comprehensive representation in non-dimensional parameters. For every *M*, spalling stress exhibits rapid escalation, reaching its peak in proximity to the edge of the anchor plate. Subsequently, it gradually diminishes to zero while moving towards the edge of the anchorage zone. Notably, a crucial observation from Figs. 6 and 7 highlights that for specific *M* values, the maximum spalling stress surpasses the maximum bursting stress. This disparity emphasizes the imperative need for meticulous consideration and heightened concern during the design phase of the anchorage zone.

3. ANALYTICAL STUDY

The investigation of the post-tensioned anchorage zone has highlighted specific areas prone to substantial tensile stresses, particularly bursting and spalling stresses, perpendicular to the direction of prestress loading. These tensile stresses pose a significant challenge due to the inherent weakness of concrete in tension. A strategic solution involves reinforcing these vulnerable regions to mitigate the adverse impact of these stresses. Various strategies have been explored to achieve this objective, encompassing the analysis of the anchorage zone with proposed reinforcement configurations, comparing them with conventional methods such as Mats or Grids, Links, Loops, Hair-pin bars, and Helices or Spiral [1]. The research extends to examining novel reinforcement configurations. Comprehensive details concerning the FE model and the intricate layouts of reinforcements are elaborated upon in the subsequent section for a comprehensive understanding.

A. FE Model incorporating proposed reinforcement configurations

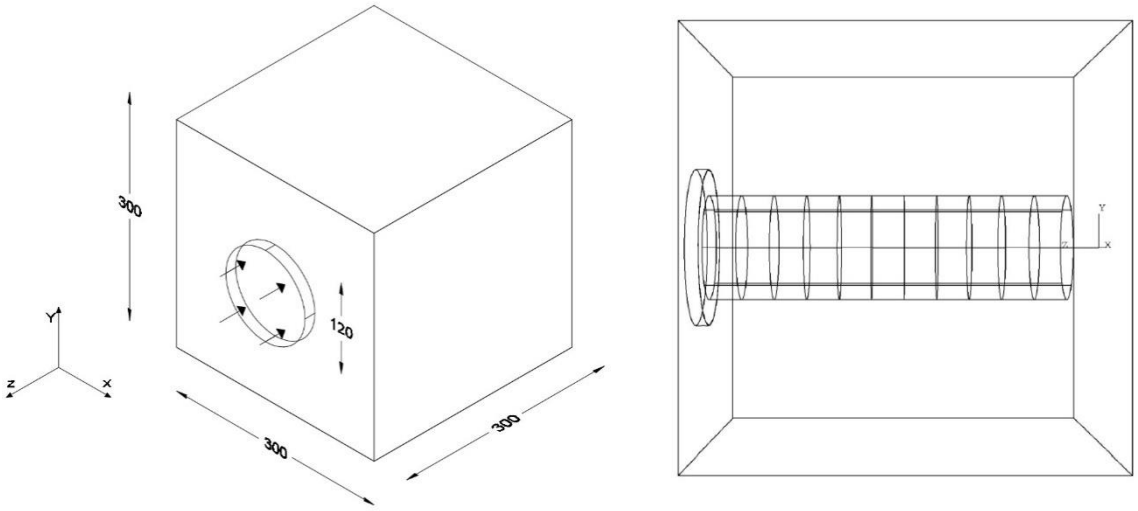

(a) (b)

Fig 8: (a) Geometry adopted for FEA and (b) Provision of RC-1 at end block

FE employs a cubical anchorage zone approach to investigate multiple reinforcement configurations. Fig. 8(a) illustrates the schematic diagram of the anchorage zone under consideration. To ensure a valid comparison among different systems, uniformity is maintained in the distribution ratio *(M)* and prestress force across all models, set at 0.4 and 1000 kN, respectively. A circular steel anchor plate, measuring 10 mm in thickness, is centrally placed on the loading surface, where an equivalent prestressing stress is applied. The steel reinforcements are modeled as wire elements with a diameter of 10 mm, and their layouts are detailed in the subsequent section. The material properties for the anchor plate, end block and reinforcement are documented in Tables II, III, and IV, respectively.

To facilitate interaction, a tie surface-to-surface constraint is enforced between the anchorage zone and the anchor plate, ensuring a secure connection. Additionally, an embedded region constraint is applied between the reinforcement elements and the anchorage zone, ensuring proper integration. Meshing of the anchorage zone and anchor plate utilizes C3D10 elements (10-node quadratic elements) with a size set at 0.05 of the anchorage zone's height. Conversely, the reinforcement bars are meshed using B31 elements (2-node beam in space), with a size set at 0.1 of the bar's length. A support mechanism is implemented on the opposite face of the loading direction, providing displacement restraint solely in the loading direction for accurate analysis of the reinforcement configurations' performance.

TABLE III: MATERIAL PROPERTIES OF CONCRETE

Density (Tonne/mm^3)	2.4×10^{-9}
Elastic:	
Young's modulus (N/mm^2)	3.1623×10^4
Poisson's ratio (μ)	0.18 0.125 0.2 0.45

TABLE IV: MATERIAL PROPERTIES OF STEEL (REINFORCEMENT)

Density (Tonne/mm^3)	7.85×10^{-9}
Elastic: Young's modulus (N/mm^2) Poisson's ratio (μ)	 2.1×105 0.3
Plastic: Yield stress (N/mm^2) 250 394	 Plastic strain 0

B. 0.012

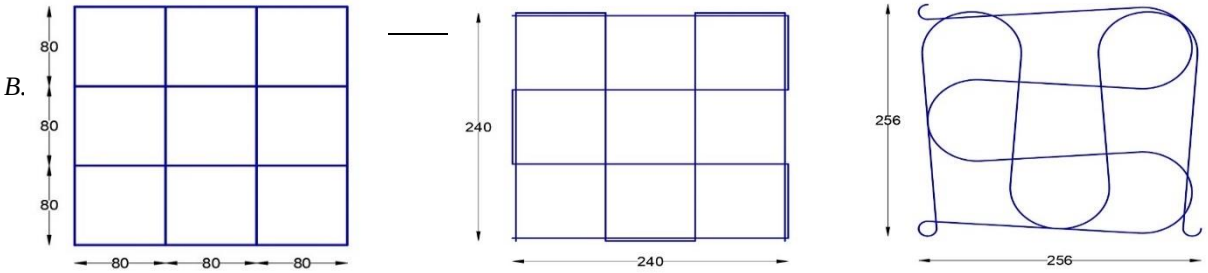

(a) Mats or grids (b) Links (c) Loops

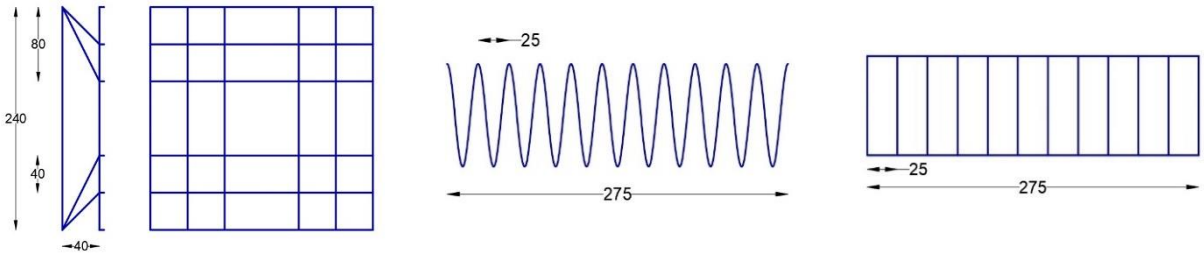

(d) Hair pin bars (e) Helices or spirals (f) RC-1

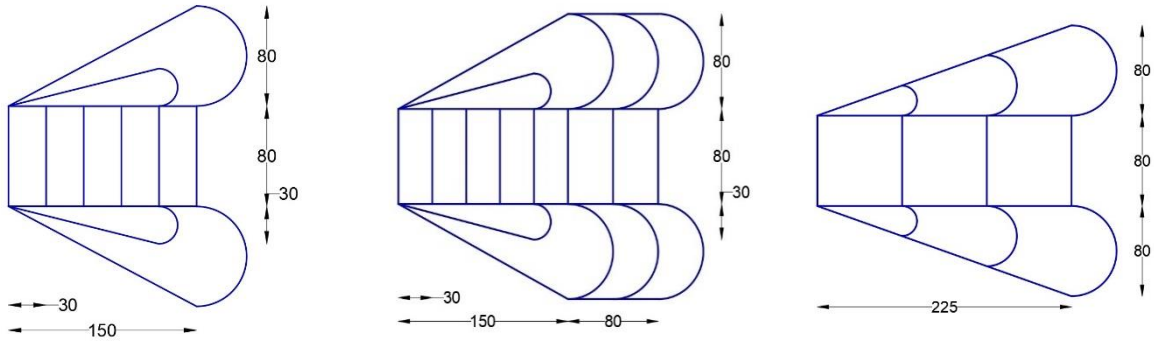

(g) RC-2 (h) RC-3 (i) RC-4

(j) RC-5 (k) RC-6 (l) RC-7

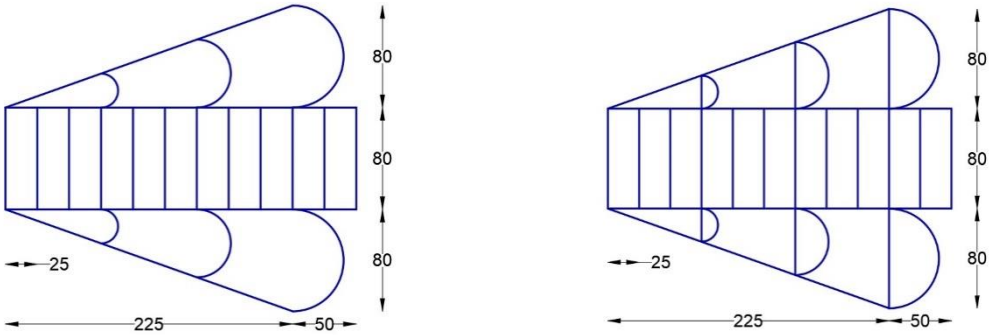

(m) RC-8 (n) RC-9

Fig 9: Geometry of reinforcement configurations (All dimensions are in mm)

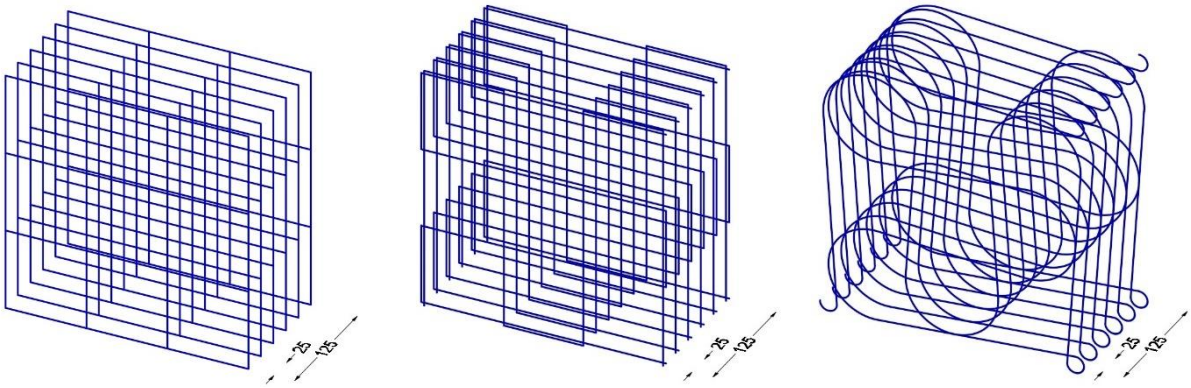

(a) Mats or Grids (b) Links (c) Loops

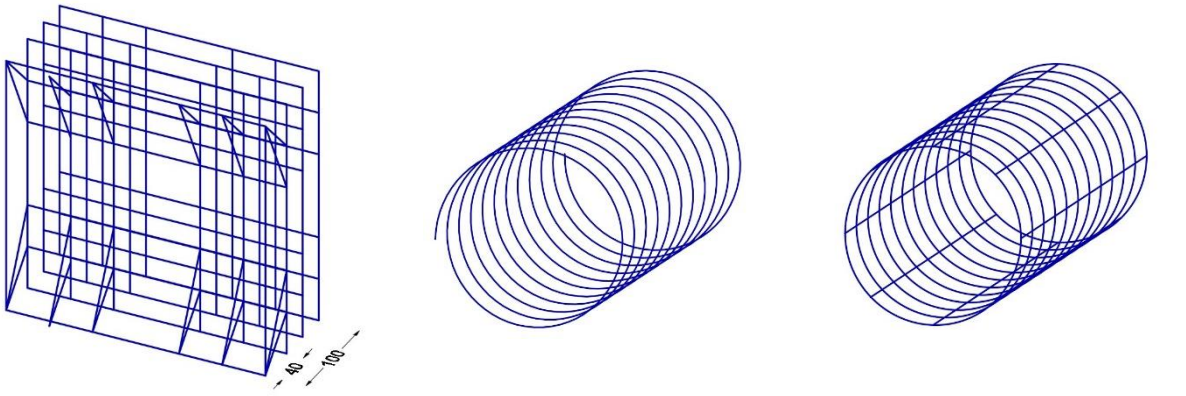

(d) Hair-pin bars (e) Helix or spirals (f) RC-1

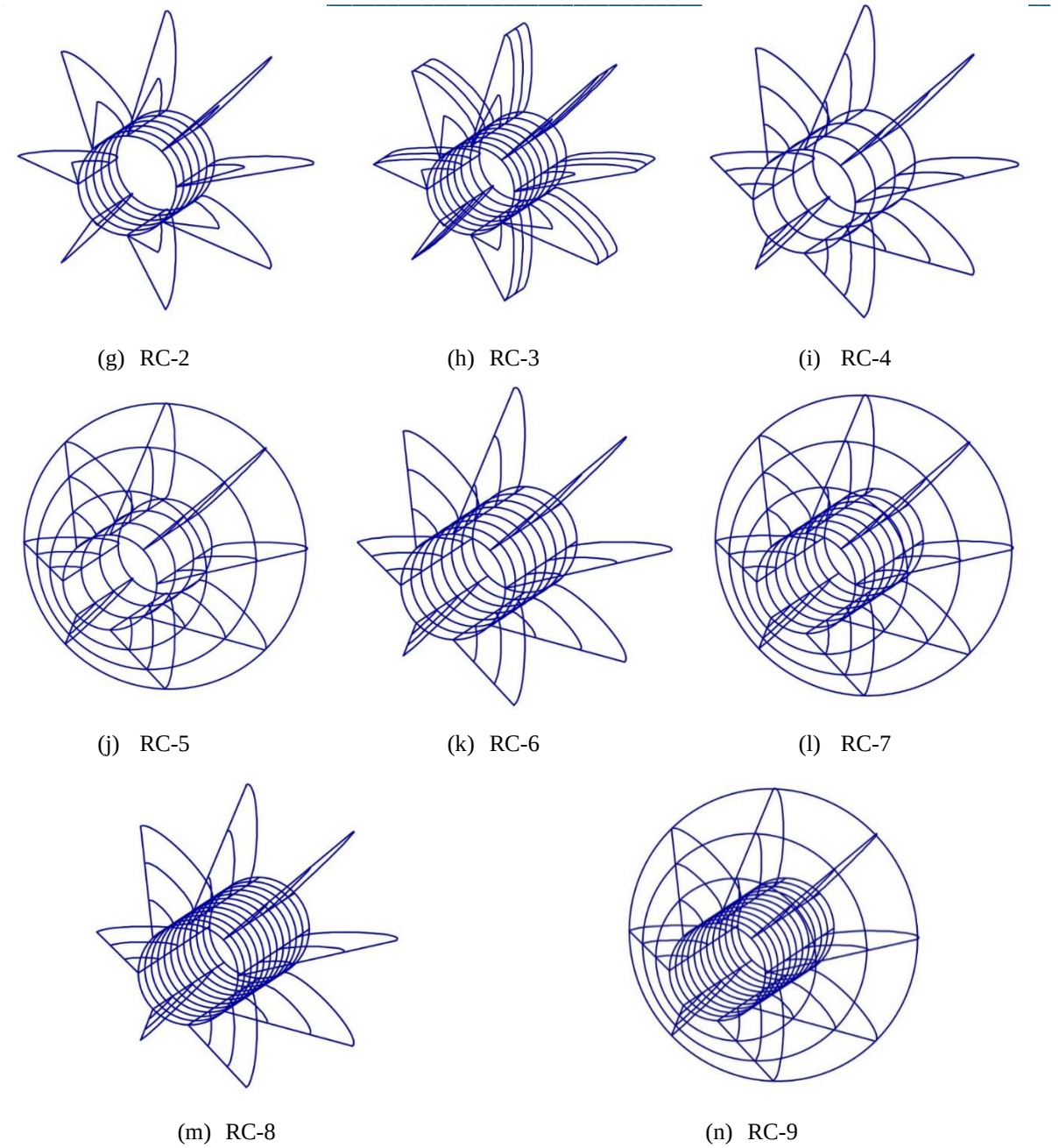

(g) RC-2 (h) RC-3 (i) RC-4

(j) RC-5 (k) RC-6 (l) RC-7

(m) RC-8 (n) RC-9

Fig 10: 3-dimensional model of reinforcement configurations (All dimensions are in mm)

Figs. 9 and 10 delineate the two-dimensional and three-dimensional representations of reinforcement configurations models, respectively. To ensure a comprehensive comparative analysis, all proposed configurations adhere to identical geometrical and material properties elucidated in the preceding section. The initial systems considered are conventional configurations, namely Mats or Grids, Links, Loops, Hair-pin bars, Helices, and Spiral. Notably, these conventional systems boast steel quantities, which, barring Helices, are uniform and exceed those of the proposed systems. It is pertinent to note that the steel quantities were predetermined, not calculated from standard equations.

In all conventional systems, the offset of the first layer of rebar stands at 30 mm from the loading surface, whereas Helices initiates precisely behind the anchor plate, a detail depicted in Fig. 8(b) showcasing one of the anchorage systems within the anchorage zone. The configurations showcased in Fig. 9 exhibit similar geometries, characterized by circular rings along the tendon path around the cable duct. These rings support

straight horizontal bars in the circumferential direction, interconnected by semi-circular arches and inclined straight bars. The alignment of these bars follows the radial direction concerning the centroidal axis of the anchorage zone. Notably, this study excludes the cable duct to focus solely on the reinforcement aspects.
It's essential to highlight that these geometries were meticulously determined, taking into account the workability of the concrete mixture and the maximum aggregate size, set at 10 mm due to the smaller size of the chosen anchorage zone. Subsequent modifications to be applied to further reinforcement configurations are rooted in the insights gleaned from the results of the previous configurations, a detailed discussion of which follows in the subsequent section.

C. Results and Discussion

The bursting stress data shown in Figs. 11-14 is gathered along the centroidal axis spanning the length of the anchorage zone. The zone is characterized by diverse reinforcement configurations as depicted in Fig. 9. On the other hand, spalling stress data in Figs. 15-18 is derived from the vertical centroidal axis situated on the loading surface. Each of these graphs encompasses data points from the anchorage zone without any reinforcement. This comprehensive approach is undertaken to assess the influence and effectiveness of various reinforcement configurations on both bursting and spalling stresses.

Fig. 11 illustrates the variation in bursting stress within the anchorage zone, both in the absence of reinforcement and with various conventional and proposed reinforcement configurations. The analysis indicates an initial burst initiation between 40-50 mm from the loading face, followed by a sharp rise to a peak value of 3.82 MPa at 105 mm from the loading face. Subsequently, the stress gradually diminishes to a minimum of 0.98 MPa at the zone's end in without reinforcement.

Comparatively, all presented reinforcement configurations exhibit analogous bursting stress patterns, with reductions of 28-34% in maximum stress achievable due to consistent patterns along the tendon path. This reduction is instrumental in controlling bursting stress. Moreover, an average reduction of 16-20% in stress is observed across the entire length. In this context, conventional reinforcement configurations manifest spalling stress patterns like those found in unreinforced anchorage zones. A noteworthy exception is observed with Hair-pin bars, which offer a modest reduction of 5-6%, as detailed in Fig. 15. This achievement can be attributed to the provision of Hair-pin links near the loading face of the anchorage zone.

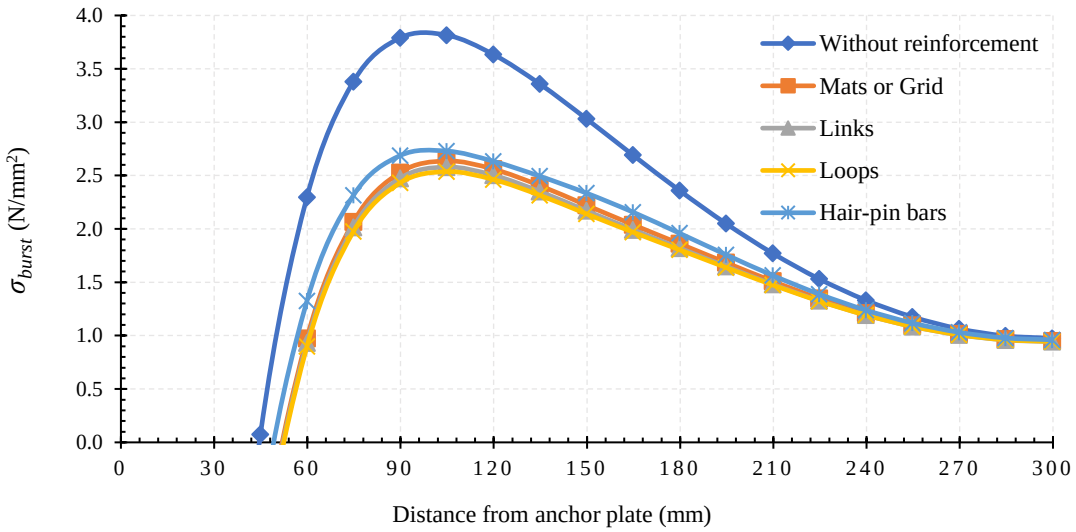

Fig 11: Bursting stress along tendon path for first group of reinforcement

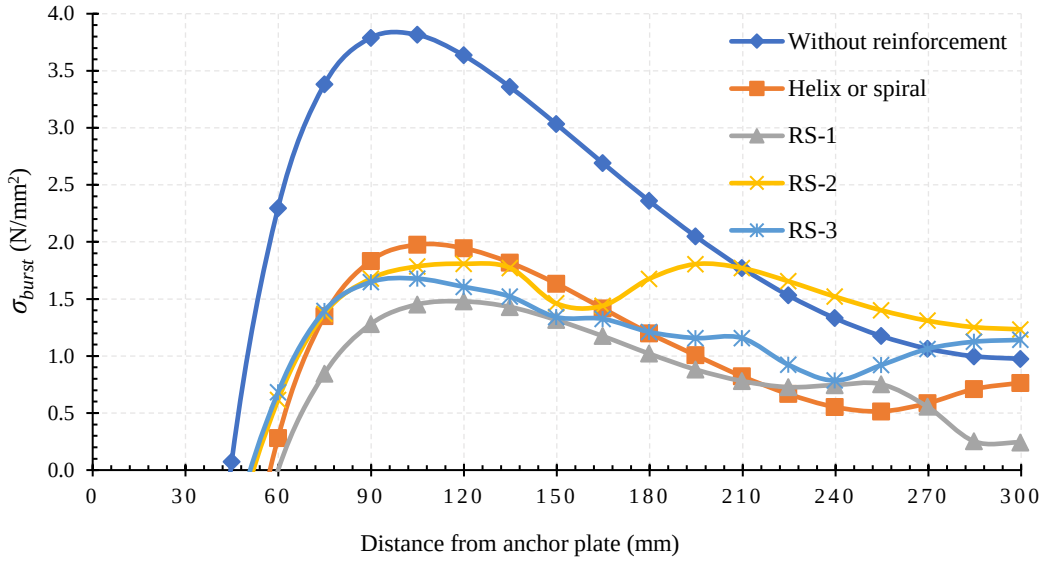

Fig 12: Bursting stress along tendon path for second group of reinforcement

Fig. 12 delineates the bursting stress characteristics derived from helical and proposed reinforcement configurations. Helical exhibits an exceptional reduction in bursting stress, outperforming conventional systems with a remarkable decrease of 48.22%. This efficacy is attributed to the spiral geometry's superior control, dispersing stress radially along the tendon path. However, the same spiral layout proves ineffective in minimizing spalling stress, as evidenced in Fig. 16. Analyzing the performance of traditional reinforcements at anchorage zone, it becomes apparent that there is a pressing need for viable reinforcement configurations capable of effectively managing both stresses.

To tackle this challenge, numerous attempts have been made, as illustrated in Figs. 9 and 10. Among these designs, RC-1, RC-2, & RC-3 are noteworthy. Fig. 12 presents the bursting stress data for these systems, highlighting the significant reduction achieved by RC-1, which mitigates 62% of the maximum bursting stress. Notably, this system also succeeds in reducing the maximum spalling stress by 16%, facilitated by the incorporation of horizontal straight bars positioned atop the circular ring. These bars impede the transfer of stress from the tendon path to the loading surface, enhancing the overall stress control efficacy.

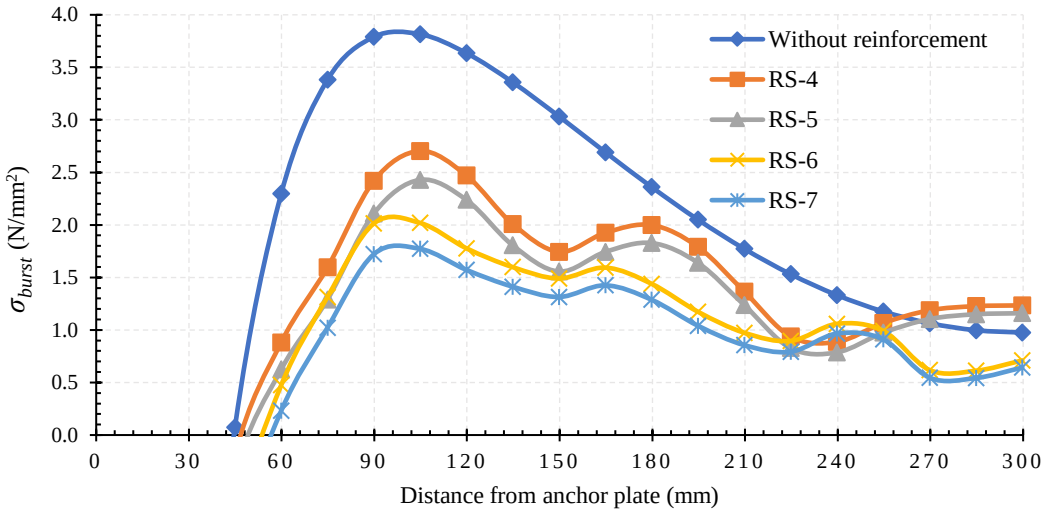

Fig 13: Bursting stress along tendon path for third group of reinforcement

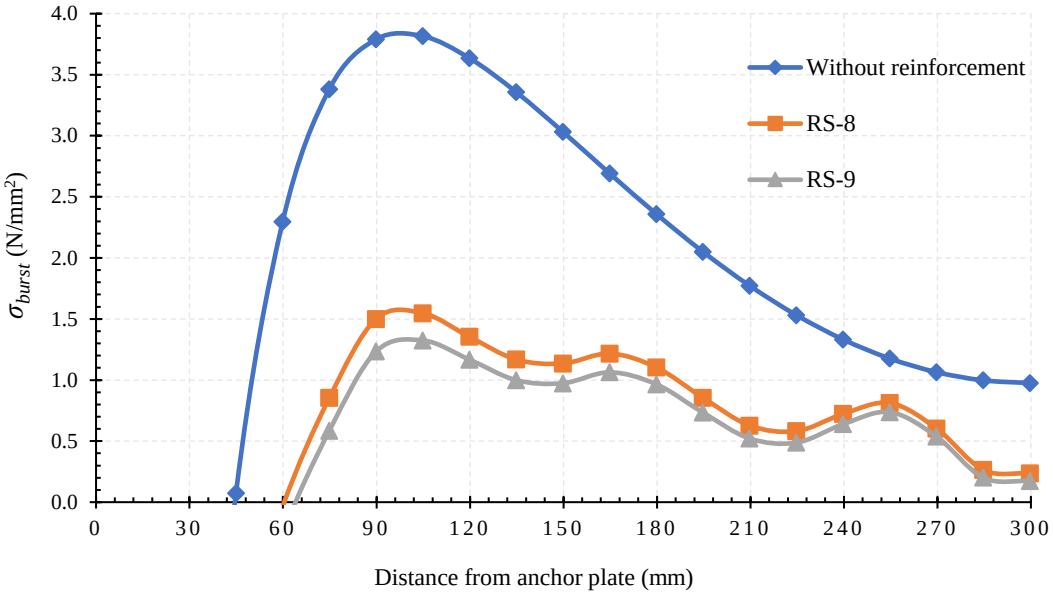

Fig 14: Bursting stress along tendon path for fourth group of reinforcement

RC-2 and RC-3 exhibit a similar stress variation pattern in the initial half of the length, owing to their analogous layouts as depicted in Figs. 9 and 10. Both configurations achieve a substantial reduction in maximum bursting stress, approximately 53-56%. However, their control along the entire length is comparatively limited when compared to helical and RC-1. Notably, RC-2 experiences a sudden increase in bursting stress beyond the initial half-length due to its configuration covering only half of the zone. This issue is addressed by incorporating two additional circular rings and a semi-circular arch, as illustrated in Figs. 9 and 10.

Furthermore, the inclined bar arrangements in RC-2 and RC-3 result in a significant decrease of around 33-35% in maximum spalling stress, a feat unattainable with conventional methods, as demonstrated in Fig. 16. This highlights the effectiveness of the inclined bar layout in minimizing spalling stress, showcasing a distinct advantage over traditional approaches.

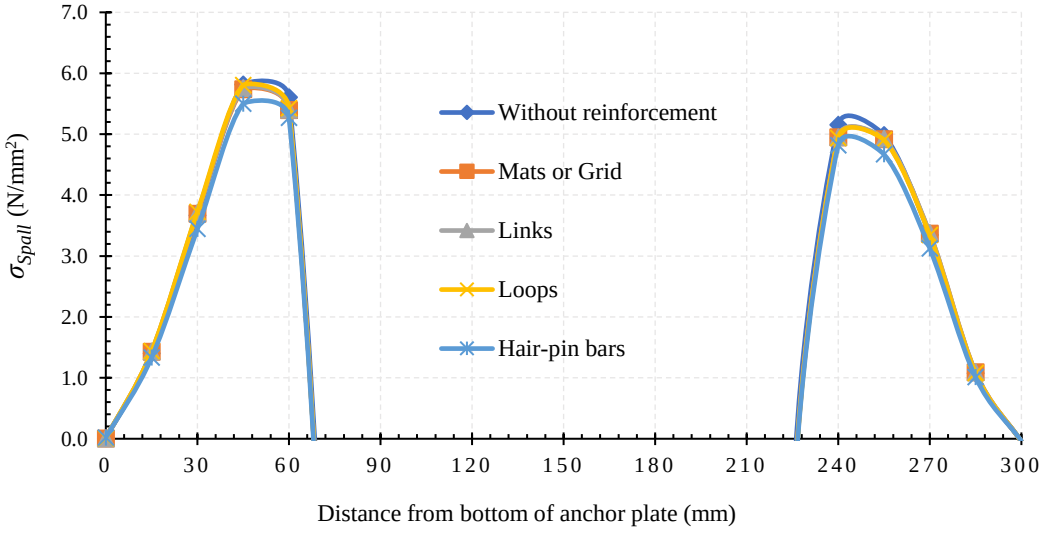

Fig 15: Spalling stress along loading face for first group of reinforcement

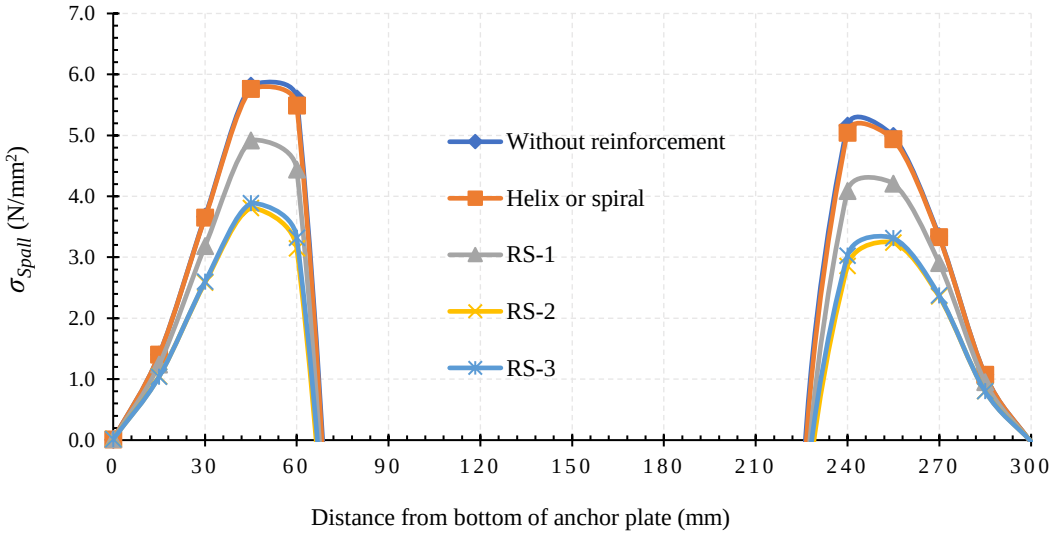

Fig 16: Spalling stress along loading face for second group of reinforcement

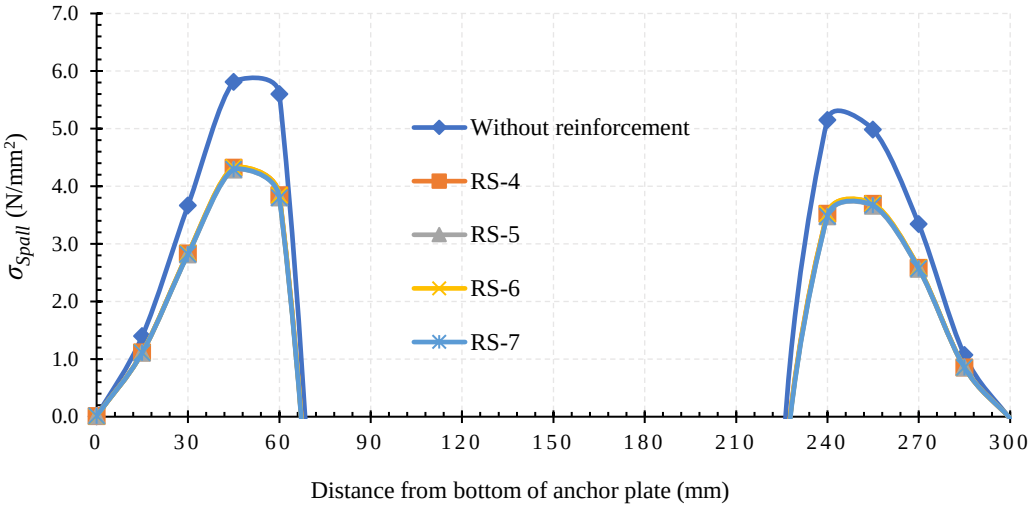

Fig 17: Spalling stress along loading face for third group of reinforcement

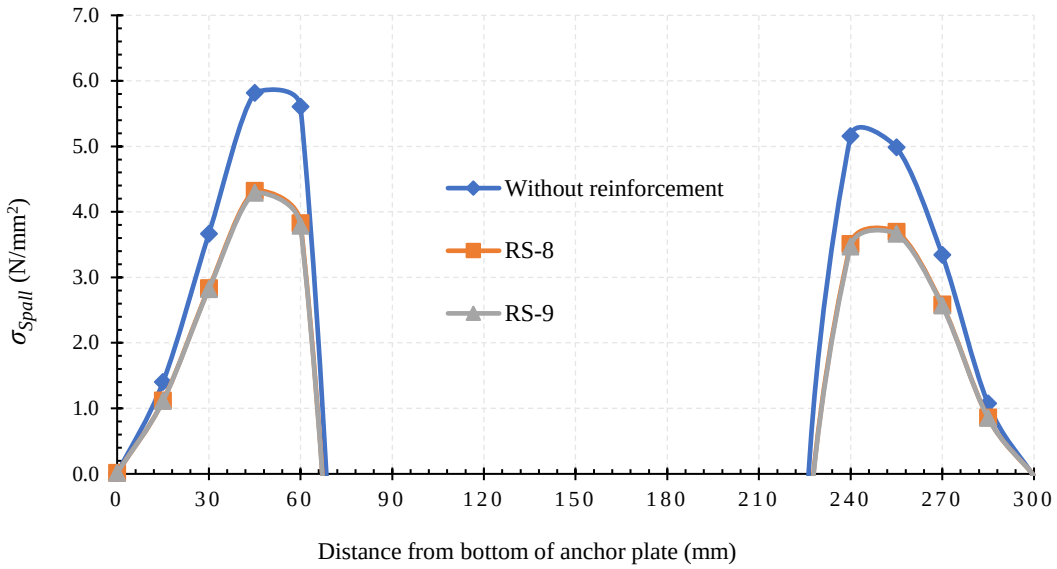

Fig 18: Spalling stress along loading face for fourth group of reinforcement

In the case of RC-2 and RC-3, a modification was introduced to alleviate congestion in the initial portion of the small anchorage zone. This adjustment involved the provision of a single inclined bar, replacing two bars on top of the circular ring, for a larger length, as depicted in Fig. 9. Fig. 13 illustrates the comparative efficacy of RC-4 and RC-5 concerning bursting stress. Both configurations share a similar layout, except for RC-5, which features three additional outer rings positioned atop a straight inclined bar. These extra components enhance bursting stress reduction, with RC-5 outperforming RC-4. An interesting observation is the absence of a gradual decline in bursting stress following the peak, attributed to the larger spacing between circular rings. However, efforts to mitigate this fluctuation were made by incorporating an extra circular ring between the existing rings for RC-6 and RC-7, as depicted in Figs. 9 and 10. This modification successfully reduced the rise and fall phenomenon in bursting stress along the length, contributing to maximum stress reductions of approximately 47% and 53% for RC-6 and RC-7, respectively.

In contrast, similar trends are observed in spalling stress variations, as shown in Fig. 17. This consistency arises from the identical layout atop the circular ring across all systems, significantly responsible for mitigating spalling stress. While not as prominent as in RC-2 and RC-3, substantial spalling stress reduction of 25-27% is achieved. Notably, the spacing between two circular rings plays a pivotal role in controlling bursting stress. To optimize this, RC-8 and RC-9 were developed as modifications of RC - 1-7, featuring closely spaced circular rings. Fig. 14 demonstrates that these modifications yield remarkable reductions of approximately 59% for RC-8 and 65.3% for RC-9, surpassing previous designs. Moreover, an average stress reduction of 59.66% along the tendon path is achieved. Additionally, these systems offer the advantage of initiating bursting stress at a significantly greater distance compared to the unreinforced anchorage zone. Similar trends are observed between RC-8 and RC-9, as well as between RC-4 and RC-5, and RC-6 and RC-7, owing to the presence of extra outer rings. Spalling stress variation, as shown in Fig. 18, mirrors the trends observed in the anchorage zone with RC-4, 5, 6, and 7 configurations.

D. Recommendations

Based on the current analysis of anchorage zones employing novel reinforcement configurations, the subsequent recommendations are formulated for the efficient management of bursting and spalling stresses:

Recommendations for Bursting Stress Control:

- Employing helices or spiral is recommended due to their superior effectiveness in controlling bursting stress, achieving an efficiency of 49%.

- In the case of narrow anchorage zones, helices or RC-1 configurations are preferable, exhibiting a remarkable 62% efficiency in bursting stress control.
- Furthermore, when there is ample space available for accommodating additional reinforcement, opting for any of the proposed reinforcement configurations proves advantageous. These systems outperform conventional methods such as Mats, Grids, Links, and Loops, as well as Hair-pin bars, requiring lesser steel reinforcement while ensuring effective stress management.

**Note: Prefer any reinforcement configuration keeping in mind two parameters, the workability of concrete and maximum size of aggregate.*

Recommendations for Spalling Stress Control:

Practicing conventional reinforcement strategies in the anchorage zone exhibit limited efficacy in spalling stress mitigation, with only hair-pin bars demonstrating marginal control, which is nevertheless insufficient.

- In scenarios where adequate space permits the installation of multiple inclined straight bars within the initial region of the anchorage zone, RC-2 and RC-3 display optimal performance by achieving maximum (around 33%) spalling stress control.
- Conversely, in situations where space constraints hinder the placement of multiple inclined bars, RC-4, RC-5, RC-6, RC-7, RC-8, and RC-9 emerge as preferable choices, playing a pivotal role in significantly mitigating spalling stress (around 26%).

Optimizing reinforcement involves strategically selecting larger diameters for circular rings placed in critical regions, particularly within the critical range spanning from $0.15l$ to $0.65l$ from the loading face, where bursting stress is notably significant. In this crucial area, circular rings can be positioned in close proximity to enhance the concrete workability and accommodate the maximum aggregate size. Additionally, the control of spalling stress can be markedly improved by incorporating a higher number of inclined straight bars, ensuring an effective stress dissipation mechanism. All proposed reinforcement configurations are meticulously arranged at minimal distances to form a compact anchorage zone, aligning with the adopted design paradigm.

Modifications should be undertaken by adjusting the spacing of rebar according to the dimensions of the anchorage zone, ensuring an optimized layout tailored to the specific size requirements. Furthermore, alterations in the diameter of the circular rings must be precisely calibrated based on the prescribed clear concrete cover from the cable duct, adhering to industry standards and design specifications. Importantly, similar to Helices or Spiral, RS - 1-9 can be seamlessly manufactured within industrial settings alongside compatible anchorage devices, streamlining the construction process.

5. CONCLUSIONS

In the comprehensive evaluation of various steel configurations implemented within the anchorage zone, encompassing both conventional frameworks such as Mats or Grids, Links, Loops, Hair-pin bars, Helices or Spiral, alongside the innovative reinforcement configurations, several key technical conclusions are drawn from this study:

- Bursting stress emerges as a critical concern within the specialized length segment between $0.15l$ to $0.65l$ from the loading face, while spalling stress reaches its pinnacle in the proximity of the anchor plate edge, escalating sharply.
- In comparison with plain helix or spiral steel configuration, RC-2 and RC-3 exhibit optimum performance, achieving maximum spalling stress reduction (around 33%), whereas in cases where spatial constraints limit the deployment of multiple inclined bars, RC-4, RC-5, RC-6, RC-7, RC-8, and RC-9 stand out as preferred choices, significantly mitigating spalling stress (average 26%).
- In scenarios involving confined anchorage zones, the utilization of helices or RC-1 configurations is recommended due to their superior effectiveness. These configurations demonstrate exceptional efficiency, achieving a significant 62% reduction in bursting stress, making them optimal choices in such constrained settings. This approach results in a substantial reduction (approximately one-fourth) in the steel provision typically practiced conventionally as anchorage zone configurations.

- Circular steel rings strategically positioned around the tendon path prove instrumental in effectively controlling bursting stress. This radial dispersion mechanism is notably leveraged by Helices, RC-1, RC-2, RC-3, RC-6, RC-7, RC-8, and RC-9, yielding commendable results. Moreover, the study underscores the impact of the distance between circular rings on the efficient management of bursting stress, emphasizing the importance of closely positioning these rings while ensuring compatibility with concrete workability.

NOTATION AND NOMENCLATURE

l	Length of anchorage zone
b	Width of anchorage zone
h	Height of anchorage zone
b'	Width of square anchor plate
h'	Height of square anchor plate
σ_{burst}	Bursting stress
σ_{Spall}	Spalling stress
σ_{avg}	Average stress (Prestress Force / Cross-sectional area of anchorage zone)
M	Distribution ratio (Height or diameter of anchor plate / Height of anchorage zone)
RC	Reinforcement Configuration
μ	Poisson's ratio
RC-1	12 Circular rings with 8 horizontal straight bars
RC-2	6 Circular rings with 2 inclined straight bars accompanied by 2 arches
RC-3	8 Circular rings with 2 inclined straight bars accompanied by 4 arches
RC-4	4 Circular rings with single inclined straight bar accompanied by 3 arches
RC-5	4 inner and 3 outer rings with single inclined straight bar accompanied by 3 arches
RC-6	8 Circular rings with single inclined straight bar accompanied by 3 arches
RC-7	8 inner and 3 outer rings with single inclined straight bar accompanied by 3 arches
RC-8	12 Circular rings with single inclined straight bar accompanied by 3 arches
RC-9	12 inner and 3 outer rings with single inclined straight bar accompanied by 3 arches

REFERENCES

[1] Krishna Raju, N. (2018). "Prestressed concrete." Sixth edition, McGraw Hill Education (India) Pvt. Ltd. Chennai, Chapter 10
[2] Zhou, L.Y., Z. Liu, and Z. Q. He. (2017). "Elastic-to-plastic strut-and-tie model for concentric anchorage zone." Journal of Bridge Engineering, Vol. 22, pp. 04017070-1-16
[3] Guyon, Y. (1953). "Prestressed concrete." Contractors Record Ltd, Chapter 6, London
[4] Yettram, A. L., and K. Robbins. (1969). "Anchorage zone stresses in axially post-tensioned members of uniform rectangular section." Magazine of Concrete Research, Vol. 21, pp. 103-112
[5] Yettram, A. L., and K. Robbins. (1970). "Anchorage zone stresses in post-tensioned uniform members with eccentric and multiple anchorages." Magazine of Concrete Research, Vol. 22, pp. 209-218

[6] Iyengar, K. T. S., and C. V. Yogananda. (1966). "A Three-dimensional stress distribution problem in the anchorage zone of a post-tensioned concrete beam." Magazine of Concrete Research, Vol. 18, pp. 75-84

[7] Zielinski, J., and R. E. Rowe. (1960). "An investigation of the stress distribution in the anchorage zone of post-tensioned concrete member." Research Report No. 9, Cement and Concrete Association, London

[8] Gupta, P. K., and R. N. Khapre. (2008). "A study on development on stresses in anchorage zone using parallel processing." Asian Journal of Civil Engineering (Building and Houssing), Vol. 9, pp. 47-59

[9] IS 1343 : 2012 Indian standard Code of practice for prestressed concrete. Second revision., Bureau of Indian Standard, New Delhi

[10] He, Z. Q., and Z. Liu. (2011). "Investigation of bursting forces in anchorage zones: compression-dispersion models and unified design equation." Journal of Bridge Engineering, Vol. 16, pp. 820-827

[11] Zhou, L. Y., Z. Liu, and Z. Q. He. (2017). "Crack propagation and control in concentric post-tensioned anchorage zones." Journal of Bridge Engineering, Vol. 22, pp. 04017075-1-10

[12] Hou, D. W., J. L. Zhao, J. S. L. Shen and J. Chen. (2017). "Investigation and improvement of strut-and-tie model for design of end anchorage zone in post-tensioned concrete structure." Construction and Building Materials, Vol. 136, pp. 482-494